University of Wisconsin Milwaukee
UWM Digital Commons

Theses and Dissertations

May 2021

Fabrication of Double-Walled Polymeric Microspheres for Improved Bone Healing and Regeneration.

Sara Travia
University of Wisconsin-Milwaukee

Follow this and additional works at: https://dc.uwm.edu/etd

 Part of the Biomedical Engineering and Bioengineering Commons

Recommended Citation

Travia, Sara, "Fabrication of Double-Walled Polymeric Microspheres for Improved Bone Healing and Regeneration." (2021). *Theses and Dissertations*. 2739.
https://dc.uwm.edu/etd/2739

This Thesis is brought to you for free and open access by UWM Digital Commons. It has been accepted for inclusion in Theses and Dissertations by an authorized administrator of UWM Digital Commons. For more information, please contact scholarlycommunicationteam-group@uwm.edu.

FABRICATION OF DOUBLE-WALLED POLYMERIC MICROSPHERES

FOR IMPROVED BONE HEALING AND REGENERATION

by

Sara Travia

A Thesis Submitted in

Partial Fulfillment of the

Requirements for the Degree of

Master of Science

in Engineering

at

The University of Wisconsin-Milwaukee

May 2021

ABSTRACT

FABRICATION OF DOUBLE-WALLED POLYMERIC MICROSPHERES
FOR IMPROVED BONE HEALING AND REGENERATION

by

Sara Travia

The University of Wisconsin-Milwaukee, 2021
Under the Supervision of Professor Priyatha Premnath

The purpose of this study was to fabricate double-walled microspheres loaded with specific drugs to improve bone healing properties. The proposed microsphere design consists of hydroxyapatite-loaded poly(L-lactic acid) (PLLA) as the core layer and cobalt (II) chloride-loaded poly(DL-lactic–co-glycolic) (PLGA) as the shell layer. Cobalt (II) chloride and hydroxyapatite were the chosen drugs because they have previously shown to aid chondrogenesis and osteogenesis, respectively. The morphology, layer identification, and elemental composition of the prepared microspheres were evaluated using a combination of scanning electron microscopy (SEM), energy dispersive X-ray spectroscopy (EDS), 3D laser microscope, and selective dissolution techniques. With the help of these characterization methods, the shell and core layers identified as PLGA and PLLA, respectively, and the surface appeared porous/smooth for small particles and porous/rough for larger particles (>400um). Lastly the presence of hydroxyapatite and cobalt(II) chloride were identified throughout both the shell and core layers.

© Copyright by Sara Travia, 2021
All Rights Reserved

To

my mother,

my sisters,

my Matthew,

and the rest of my family.

TABLE OF CONTENTS

LIST OF FIGURES

LIST OF TABLES

LIST OF ABBREVIATIONS

HA	Hydroxyapatite
SEM	Scanning Electron Microscope
EDS	Electron Dispersive X-ray Spectroscopy
MW	Molecular Weight
$CoCl_2$	Cobalt (II) Chloride
W/O/O/W	Water-in-Oil-in-Oil-in-Water
FIB	Focused Ion Beam

ACKNOWLEDGEMENTS

First and foremost, I want to thank my advisor, Dr. Priyatha Premnath, for recognizing my potential to move forward with this thesis topic. Dr. Premnath provided great support, encouraged me to get trained on various characterization instruments and protocols, was flexible around my full-time work schedule (making meeting times work), and most importantly, taught me so much about bone and its healing process.

A tremendous thanks to Chloe Hotze, an undergraduate student currently attending UW-Milwaukee who is focused in the Materials Engineering field. Chloe provided valuable research support but most importantly assisted with sample preparation and collection. With the fabrication protocol being lengthy, it was a huge help to have Chloe's reliable support throughout the fabrication process.

A final thanks to Dr. Steven Hardcastle who provided valuable input on various characterization techniques applicable for this project. Dr. Hardcastle trained me on SEM/EDS equipment and the 3D laser microscope. This training was not only valuable for supporting my research but also added a skillset to be used for my professional career.

1. Introduction:

1.1 Overview of the process of bone healing after an injury:

When a bone fracture happens, there are typically three stages of healing; 1) the inflammatory phase, 2) the repairing phase, and 3) the bone remodeling phase [2,3,23]. A detailed figure of these stages is shown below (Fig 1).

The inflammatory phase, also known as fracture hematoma formation (Fig 1, a), immediately occurs after a fracture. Approximately 48 hours after the injury, blood vessels torn by the fracture release blood. This blood starts to clot and forms a fracture hematoma which ultimately diminishes blood flow to the bone causing tissue hypoxia, formally known as ischemia. With the bone cells having limited oxygen supply due to the hypoxic environment, cells and tissues around the fracture start to die [2,3]. From there, cytokines act to stimulate essential cellular biology at the site, attracting macrophages, monocytes, and lymphocytes [23]. These cells work together to remove necrotic tissue and secrete cytokines like vascular endothelial growth factor (VEGF) to stimulate healing at the site [23]. VEGF promotes the development of endothelial cells to induce vascular invasion under hypoxia [27] and ultimately aid with angiogenesis at the site [23]. While vascularity continues to be regained, mesenchymal stem cells (MSC) are recruited to the area and begin to differentiate to fibroblasts, chondroblasts, and osteoblasts [2,12,18,23]. As a result, chondrogenesis begins to occur, forming a soft collar of cartilage tissue at the broken ends of the bones [2,3], with a surrounding hyaline cartilage sleeve [23]. These growths are known as fibrocartilaginous calluses (Fig. 1, b) and their purpose is to stabilize the fracture [2,3]. Over the following weeks, cartilaginous calluses begin to undergo endochondral ossification [2,12,23]. During this phase, cartilaginous calluses are converted into a bony callus made of

spongy bone (Fig. 1, c) which then replace the tissue callus [2,23]. As newly formed blood vessels continue to proliferate, more MSCs migrate to the injured site where the bony callus undergoes coupled remodeling [23]. The continued migration of osteoblasts and osteoclasts drives the remodeling, resulting in regeneration of the normal bone structure [23] as shown in Fig. 1, d. This entire healing process can last anywhere between several months to several years, depending on the individual. To give an idea of time allocated for each healing phase of a human bone; the inflammatory phase lasts 1 to 5 days, the repairing phase lasts for 2-4 weeks, and the bone remodeling phase lasts for months to years [3,23].

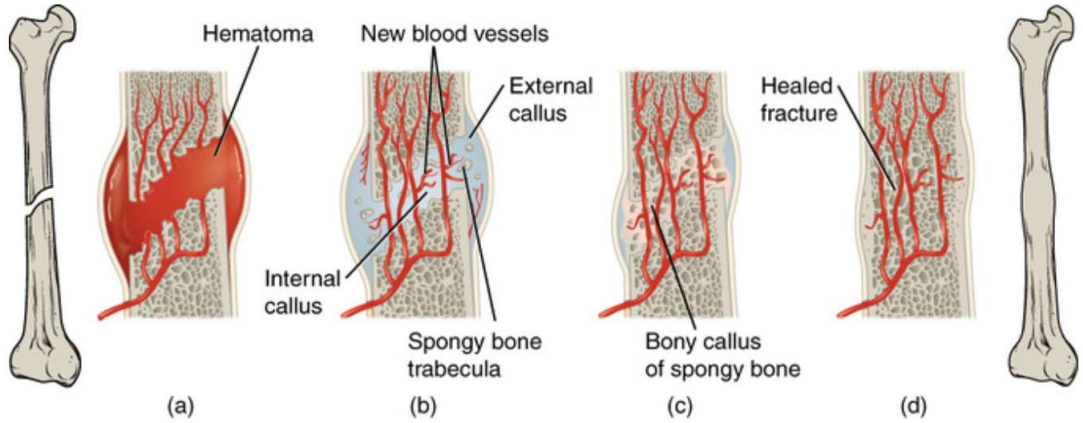

Figure 1. The healing of a bone fracture follows a series of progressive steps: (a) A fracture hematoma forms. (b) Internal and external calli form. (c) Cartilage of the calli is replaced by trabecular bone. (d) Remodeling occurs [2].

1.2 Enhanced bone healing through biomaterials

Successful repair of large bone fractures due to traumatic injury remains a clinical challenge. After a fracture occurs, the body immediately takes action to try to repair the damaged site. Although bone possesses repair capacity, it is often insufficient to overcome large bone loss [25]. For cases like these, surgical intervention is typically required to either aid the bone healing process or replace the fractured bone. Clinical approaches involve the use of bone-grafts [24,25] the application of growth factors [25], or implantation of bone fixation devices [4,24]. These

approaches utilize biomaterials that can be classified into two groups: bio-inert and biodegradable materials [24]. Autologous bone grafting is considered the gold standard because it possesses all the characteristics necessary for new bone growth [4,24,25]. However, there are limitations and concerns of this approach such as, limited bone supply, donor site morbidity, anatomical, structural and surgical limitations and increased bone resorption during healing [24,25]. The use of synthetic grafts made with osteoinductive growth factors such as recombinant human bone morphogenetic protein 2 (rhBMP2) is another approach. Unfortunately, large amounts of growth factors are needed to induce bone regeneration, and delivery of these large amounts has led to production of antibodies and other adverse effects [25]. Thus, alternative solutions, such as bio-inert biomaterials, are still widely used and have shown to be clinically partially successful for fracture fixation treatments. Issues commonly arise with these bio-inert materials, for example, they must be surgically implanted which not only increases hospitalization time and health care cost but also raises chance of infection and complications [4,24]. Also, due to the difference between the mechanical properties of these materials and the natural bone, the healing is often disrupted when stress shielding occurs. Stress shielding refers to the reduction in bone density caused by mechanical forces and loads being retained by implants instead of transferring to the healing bone. This results in unwanted bone resorption and implant loosening [24], typically requiring another surgery. Therefore, continued research to develop bone biomaterials that are biodegradable instead of bio-inert is currently a major focus. More specifically, biodegradable polymers are one of the primary and common biomaterials used for bone repair and tissue engineering. Their biodegradability and controlled degradation rates are highly beneficial for clinical applications [4,24]. In addition, polymeric materials, specifically

polymeric microspheres, are well known for their encapsulation efficiencies and play a key role in drug delivery applications.

In addition to biodegradability, there are many other properties that must be considered to develop an ideal bone biomaterial. The biomaterial should have appropriate biological and biomechanical properties (i.e. good biocompatibility) as well as good osetoinductivty [24,27]. The basic concept is that the biomaterial acts as a scaffold for the surrounding cells/tissue to invade, grow, and thus guide tissue regeneration towards new bone formation [24].

To date, researchers have devoted extensive efforts in developing biomaterials for large fracture cases. Recently, a different design approach has gained attention - designing a biomaterial to target specific cellular signaling pathways that regulate bone regeneration. As part of the repair phase, cells and tissues near the fracture become hypoxic and remain hypoxic until the newly formed blood vessels carry oxygen back into the area. In response to hypoxia, various cellular and molecular processes are activated by the body to promote and sustain tissue function [18,19]. In the case of a large fracture, specific proteins such as HIF-1α and BMPs, are recruited to aid with expression of angiogenetic factors (i.e. VEGF) which is an essential step in endochondral bone formation [18,19]. Also, MSCs are recruited to the area and as mentioned above, these begin to differentiate to fibroblasts, chondroblasts, and osteoblasts [2,12,18,23]. More recently, special attention has been paid to the interaction between bone biomaterials and MSCs [4,11,18,19]. By understanding the various signaling pathways and factors that aid with bone regeneration, biomaterials can be designed to target specific cellular pathways which will initiate other biological responses and eventually get to the end goal of improving bone healing process [11]. Most research focuses on improving bone healing by improving the osteogenesis

properties of various biodegradable biomaterials, which is the last step in the bone healing process. So far, there has been much success with improving osteogenic properties thanks to a key component; hydroxyapatite (HA), the main inorganic constituent of bone. This drug is widely used and integrated into designs to enhance bone regeneration properties [6] as well as reduce bioinert characteristics of metals to enhance osteointegration [20].

Although there has been much focus and success on developing biomaterials capable of aiding osteogenesis, there is still a lot of room to improve the healing process. Thus, the aim of this study was to fabricate a biomaterial that aids bone healing by improving chondrogenesis and osteogenesis as opposed to conventional techniques that only target osteogenesis.

1.3 Proposed Design:

In this study, we developed a double-walled microsphere loaded with two key components; HA and cobalt (II) chloride. Using two different polymers, Polylactic-co-glycolic acid (PLGA) and polylactic acid (PLLA) we created the layers following the well-established water-in-oil-in-oil-in-water (w/o/o/w) method to load the drugs. The outer layer consists of PLGA which encapsulates cobalt chloride(II). Cobalt ions have shown to create a hypoxic environment [7,22,28] which as mentioned above, is conducive for chondrogenesis. The inner layer is composed of PLLA which encapsulates HA, a key drug that aids osteogenesis [6,16,17].

PLGA was chosen as the outer layer because of its easily modified degradation properties. In addition, previous research has shown success with loading aqueous $CoCl_2$ into PLG biomaterials [22].

The purpose of this design is to allow direct injection of the microspheres to the fracture site, where the $CoCl_2$ will start to initiate hypoxia, elevating the cellular response to regain vascularity and undergo chondrogenesis. After degradation of this layer, the PLLA core layer is exposed and degradation begins, which will release HA to aid with bone formation. The purposed design is shown below in Figure 2.

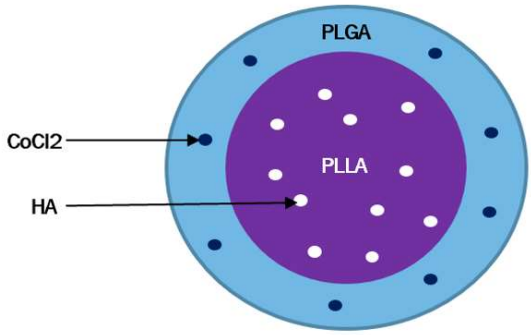

Figure 2: Simplified visual of proposed double-wall microsphere design where HA is loaded into the PLLA core and $CoCl_2$ is loaded into the PLGA shell layer.

2. Materials and methods

2.1 Materials:

Poly(L-lactic acid) (PLLA, MW 85,000-160,000), poly(DL-lactic–co-glycolic acid 50:50) (PLGA 50:50, MW 30,000-60,000), dichloromethane (DCM anhydrous), hydroxyapatite (HA <200nm particle size), cobalt (II) chloride ($CoCl_2$ anhydrous), and poly(vinyl alcohol) (PVA MW 30,000-70,000) were all purchases from Sigma-Aldrich, USA, and used without modification. ACS grade acetone, which was used for selective dissolution technique, was purchased from Fisher Chemical, USA.

2.2 Fabrication of HA and $CoCl_2$ loaded double-walled microspheres

Drug loaded microspheres were prepared using the well-established double emulsion technique; water-oil-oil-water (w/o/o/w). The two polymers, PLLA and PLGA, were chosen for this study for two reasons 1) they are incompatible with one another which aids the complete phase separation and 2) earlier research completed by Tan, E.C. (2005) found that the polymer mass ratio (i.e. 1:2, PLLA : PLGA w/w) will allow for the PLGA layer to form as the shell while PLLA forms the core layer [8]. This concept was further examined in this study.

In separate 13x100mm glass test tubes, PLGA and PLLA were separately dissolved in 1mL dichloromethane (DCM); overall concentration 10% for PLLA and 20% for PLGA, w/v. In separate beakers, 5% (w/v) HA and 5% (w/v) $CoCl_2$ solutions were prepared with water. With the single layer polymers dissolved in DCM, the drugs were added to the polymers following the single-layer hydrophilic protocol as outline in previous work [21]. 400ul of the 5% $CoCl_2$ solution was directly added to the PLGA solution and emulsified over ice at 30-W output for 10 seconds, then vortexed (American Scientific Products, Model S8223-1) on high for another 10 seconds using a sonicator (Qsonica, Model CC-188). The same steps were completed for loading the HA with the PLLA, instead adding half the amount of solution (200ul of 5% HA solution). Since the polymer mass ratio of 2:1, PLGA:PLLA, was used, 2x the volume of $CoCl_2$ solution was added to the PLGA layer. Next, the Co-PLGA solution was added drop-wise to the HA-PLLA solution using a pasteur pipette and immediately sonicated for a total of 30 seconds, completing sonication in 10 second intervals with a 5 second rest over ice in between. This time allowed for a homogenous solution to form. Next, the mixture was injected dropwise into a stirring nonsolvent bath containing 200ml of PVA solution (0.5% w/v) and left to stir at 500rpm for 3hrs. This step is key for allowing the

extraction and evaporation of DCM which allowed phase separation of PLLA and PLGA before the microparticles harden [1,8]. Next, the particles were vacuum filtered using 1um paper, rinsed three times with distilled water to remove any PVA residue, and left to dry under desiccate overnight before completing characterization. Refer to Table 1 below for the details on composition per sample set.

Table 1. Composition of each sample set

Sample	**5% HA (ul)**	**5% $CoCl_2$ (ul)**	**PLGA:PLLA ratio (w/w)**
Control	0	0	2 to 1
1	200	0	
2	0	400	
3	200	400	

2.3 Characterization Techniques:

2.3.1 *Morphology and composition study*

The morphology and composition of the microspheres were observed with the help of scanning electron microscopy (SEM), energy dispersive X-ray spectroscopy (EDS); (SEM-EDS, Jeol/Inca, Japan), and a 3D laser microscope (LEXT Olympus Model OLS4100). To capture the double walled structure as well as identify the elemental composition of each layer, a combination of these pieces of equipment were utilized. First, microspheres were cut using a microtome razer blade and then mounted to a metal stub such that the cross-sectional view was exposed. The 3D laser microscope was used to verify that the cross-sectional view was exposed prior to loading samples into the SEM-EDS instrument. Once verified, particles were coated with

palladium (Denton Vacuum, model Desk II) and analyzed using a combination of 5V and 15kV accelerating voltages.

For the sake of drug identification, several sample sets were not coated prior to completing elemental analysis. This was completed to avoid inadequate quantification of chloride since this element has a similar electron energy as the coating material, palladium (Pd = 2.696 kV and Cl = 2.621kV). The elements of interest for characterizing HA are calcium and phosphate (chemical formula: Ca_{10} $(PO_4)_6$ $(OH)_2$) while the elements of interest for cobalt (ll) chloride are cobalt (Co) and chloride (Cl).

2.3.2 *Polymer layer identification study*

For identification of the core and shell microsphere layers, a selective dissolution technique was utilized. This technique, which was also completed in other work [8], uses the different solubility properties of PLGA and PLLA to help identify if dissolution takes place when it, in this case acetone, is applied to the microsphere. Acetone was chosen for this study because PLGA is soluble in it whereas PLLA is only slightly soluble at elevated temperatures, plus it was readily available in the lab. With the help of an optical microscope (Olympus CK2, ULWCD 0.30, Japan), a cross-sectioned microsphere was imaged before, during, and after acetone treatment. With this technique, we can identify the location of PLGA by simply observing whether the particle shrinks in size (located in the shell) or the particle has a hollow center (located in the core).

3. Results and discussion

3.1 Morphology

Representative SEM images of the PLGA / PLLA double walled microspheres, using the protocol as described above, are shown in Figure 3 (a-d) below. As seen, the particles are non-fused spheres, with some having smooth porous surface morphology (Fig. 3, a-b) and others having a rough, 'wrinkly', porous surface morphology (Fig. 3, c-d). All sample batches contained particles that had both smooth and rough surfaces, with the rough typically being present on particles that were at least 400um in diameter. From Fig. 3, (d) below, many pores are present on the surface, yet the diameter of these pores vary. This will directly impact the microsphere's encapsulation efficiency because pores are the integration channel between the drugs within the polymer and the external environment. With varying pore size, it is expected that the drug release will also vary as the polymer degrades. Determining whether this release rate is acceptable will be studied in future work by directly comparing pore size to encapsulation efficiency overtime.

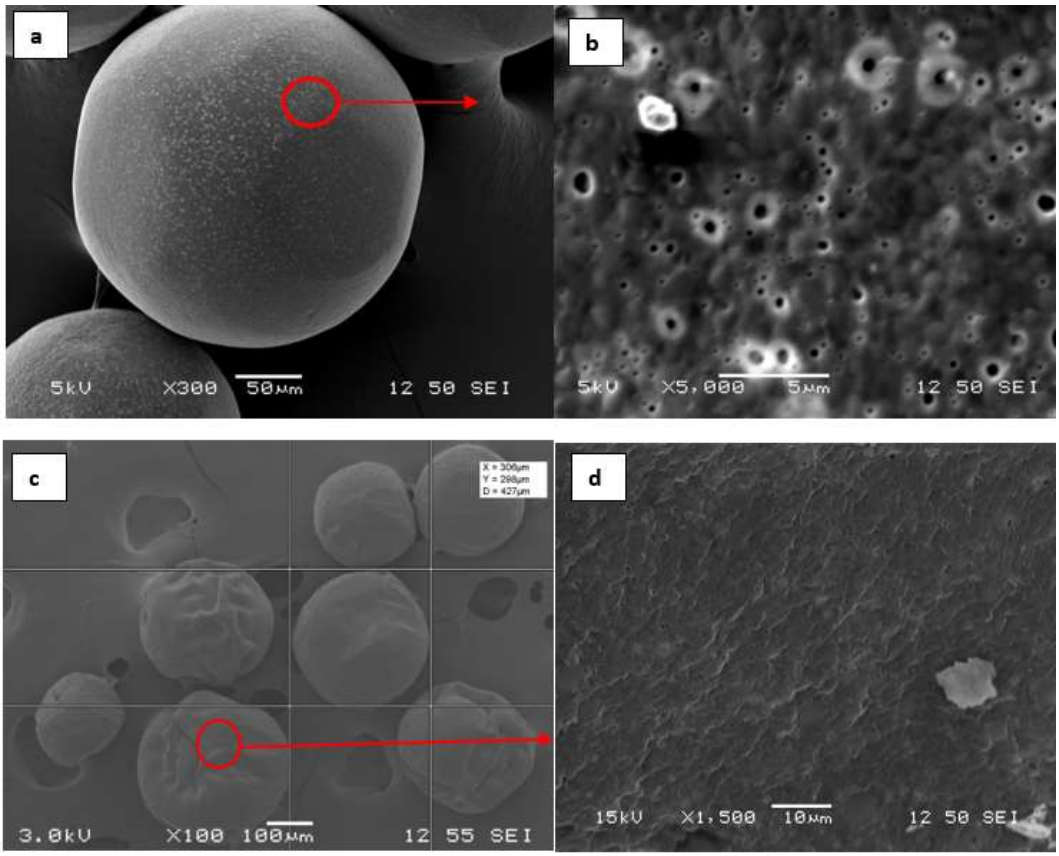

Figure 3. Sample 1 SEM images of PLGA / PLLA double walled microspheres prepared using the double emulsion technique, where (a) captures 300x SEM image of particle and (b) captures a 5,000x SEM image of the particle's smooth, porous surface.. SEM image of 'wrinkly', particles are shown in SEM with 100x and a close up the particle's rough, yet porous surface is captured in (d).

As shown in Figure 4, there is a broad range of particle sizes distributed throughout the sample batch. With the help of SEM and 3D laser microscope measuring tools, the size distribution for all batches ranged from 50-600um in diameter.

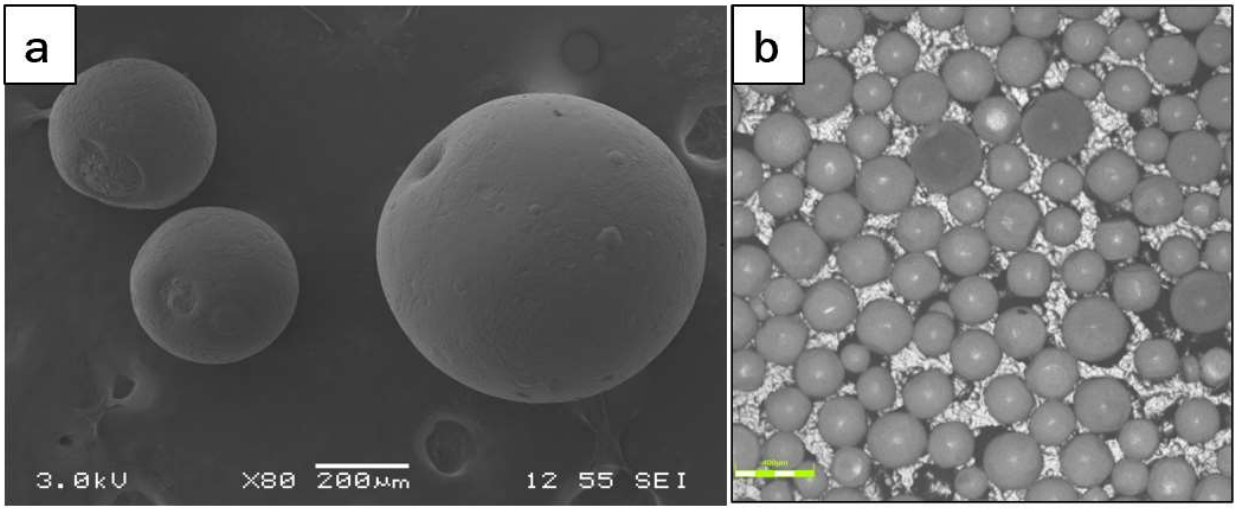

Figure 4. Prepared double-walled microspheres from sample batch 3, imaged with (a) SEM at 3kv and 80x and (b) 3D laser microscope at 5x. This figure shows the broad particle size distribution.

The variations in morphology and total size of these microspheres can be directly related to the quality and reproducibility of this fabrication protocol. The fabrication protocol used in this study is very hands-on. When adding the combined polymer layers (w/o/o) to the PVA solution to complete the emulsion (w/o/o/w), it is very important to control the flow rate of the material being added drop wise. Large droplets that form from a slow flow rate will result in the formation of large particles whereas smaller droplets that form when from a higher flow rate will result with smaller particles. Although the preparation of each batch was completed by the same person, there is much room to introduce user error. To improve reproducibility, utilizing a microfluidics device is highly recommended. These devices allow for optimal control over the flow rates of polymer solutions and emulsifying agents.

Something not captured by the SEM and 3D laser microscope images is the color and color change these particles underwent. After allowing particles to dry overnight under desiccate at room temperature, the samples with $CoCl_2$ (samples 2 &3) appeared blue in color and as temperature decreased after freezing some of the particles (-20 °C), those particles turned

pink/peach. Refer to Figure 5 for a visual comparison of the microparticle color at various temperature conditions. This color change is directly related to the chemical reaction within $CoCl_2$ which has shown to be sensitive to temperature change. By referring to cobalt chloride's equilibrium reaction shown in equation 1 below [5], we see that with a larger concentration of excess chloride present, equilibrium tends to the left, and the solution tends to be blue. In addition, at higher temperatures, the equilibrium tends to the left as well, leaving the solution blue [5].

Equation 1: $CoCl4^{2-}(aq) \leftarrow\!=\!=\!=\!=\!=\!=\!=\rightarrow Co^{2+}(aq) + 4Cl^{1-}$

Since temperature conditions were not controlled while completing SEM/EDS, it was found that all samples appeared blue either before or after loading the particles into the SEM/EDS machine. This correlates with the data presented in the next section, where a larger concentration of chloride was always identified in comparison to cobalt concentration. Also, the advantage of this color changing property that cobalt chloride presents is that it provides an additional way to identify the presence of this compound, qualitatively.

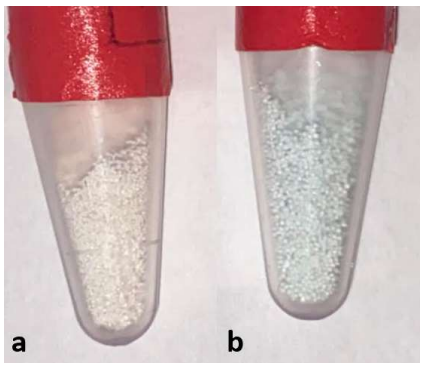

Figure 5. Color comparison of sample 2 double-walled microspheres, where a) are the microparticles that appear pink since they were just removed from the freezer and b) are microparticles that appear blue since these were stored at room temperature.

3.2 Identification of Hydroxyapatite and Cobalt Chloride Distribution

Aqueous hydroxyapatite and cobalt (II) chloride solutions were separately emulsified with PLLA and PLGA, respectively, before the two polymers were combined. From earlier trials, it was found that characterizing palladium coated microparticles interfered with identifying the presence of chloride since palladium and chloride have similar electron energies. Thus, by leaving these microparticles uncoated, all elements had a fair chance to be identified through EDS.

To study the location of HA and $CoCl_2$ compounds within the microsphere, samples with only HA (sample 1) and only $CoCl_2$ (sample 2) were fabricated and compared to the sample batch loaded with both $CoCl_2$ and HA (sample 3). The cross-sectioned microparticles (Figure 6, a-b) from each sample batch were utilized to complete elemental analysis of the shell and core layers.

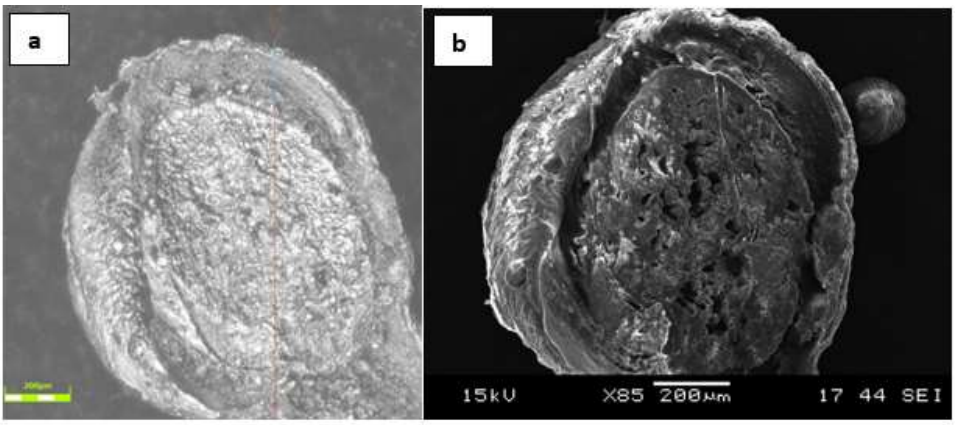

Figure 6. Cross-sectional view from sample batch 2 where (a) is the 10x 3D laser microscope image used to verify the cross-section side is exposed for optimal EDS analysis and (b) is the same, uncoated, particle imaged with SEM at 85x and 15kV.

The elemental weight percentages (wt %) were extracted from the EDS data for the shell and core layers of at least 3 different particles. Measurements were averaged and standard deviation of the sample set were calculated for each element; calcium (Ca), phosphorous (P), chloride (Cl), and cobalt (Co). The control sample did not undergo EDS analysis simply because it

was not loaded with either of the drugs. Example of the EDS results per sample is shown below in Figure 7, and the average EDS results for samples 1-3 are numerically summarized in Table 2 and graphically shown in Figure 8, a-c.

Table 2. Averaged EDS results for the shell and core layer of each sample batch and calculated standard deviation.

Average element wt %	Sample 1		Sample 2		Sample 3	
	Shell	Core	Shell	Core	Shell	Core
Ca wt% (±SD)	1.41 ± 0.51	1.74 ± 1.16			0.92 ± 0.78	2.02 ± 0.66
P wt% (±SD)	0.84 ± 0.41	1.19 ± 0.69			0.64 ± 0.51	1.01 ± 0.41
Cl wt% (±SD)			1.48 ± 0.95	5.08 ± 0.96	0.15 ± 0.30	2.63 ± 0.36
Co wt% (±SD)			0.09 ± 0.22	0.48 ± 0.76	0.00 ± 0.0	0.72 ± 1.06

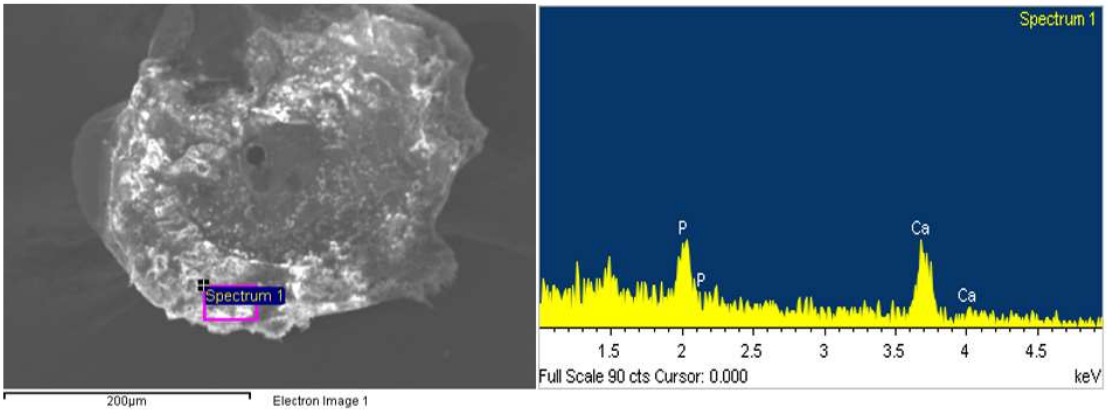

Figure 7. Example EDS output result for the shell layer of a particle sample from batch 1 (HA only). Calcium and phosphorus peaks were identified with weight percentages measured at 1.67% and 0.88%, respectively.

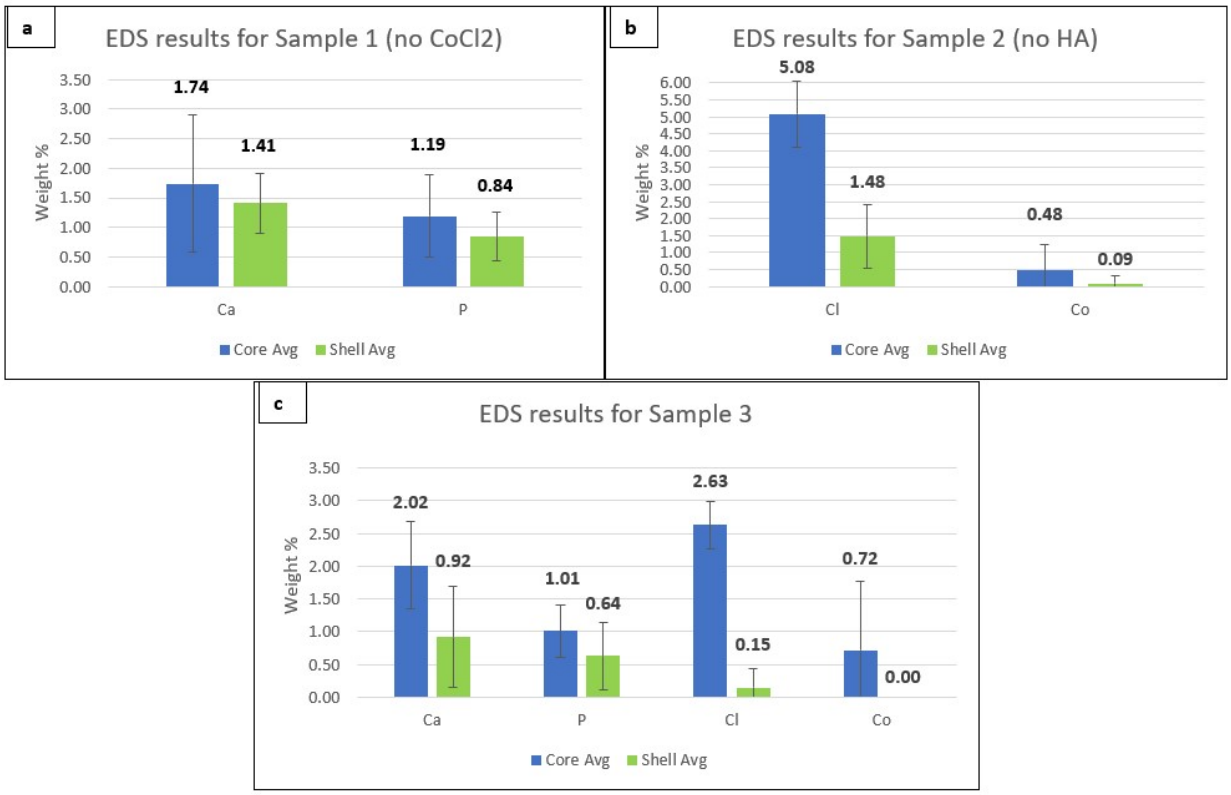

Figure 8. Graphical representation of EDS results for identifying layer distribution of HA and $CoCl_2$ loaded PLGA/PLLA double-walled microspheres using the cross-sectional view for each sample where (a) represents EDS results of sample 1 which were loaded with only HA, (b) represents EDS results of sample 2 which were loaded with only $CoCl_2$, and (c) represents the EDS results for sample 3 which were loaded with both HA and $CoCl_2$.

The error bars in Figure 8 (a-c), represent the calculated standard deviation for each sample set. These errors can be attributed to several things; 1) inadequate EDS readings due to particle movement during measurement and 2) inconsistency throughout fabrication protocol. Characterizing uncoated microparticles with SEM/EDS equipment can be challenging due to the likelihood of particles moving during an EDS capture [21]. This movement can be attributed to the accumulation of static electric charges on the particle surface, which results in many imaging problems [14]. For this reason, particles are typically coated with a conductive metal (i.e. palladium, gold, etc) to reduce thermal damage and improve the secondary electron signal required for topographic examination in the SEM [13]. Thus, future studies should consider sputter coating particles with a conductive material that have large differences in electron energy

values compared to Ca, P, Cl, and Co. This will prevent the particles from moving during EDS measurements as well as allow for all elements to be cleanly quantified. The second reason of high standard deviations can be attributed to inconsistencies of the fabrication protocol. In addition to the limited reproducibility, as mentioned above, the technique of using a blade to cut the microparticles is not only tedious, but also has potential to drag the drugs located in the shell to the core (i.e. cross contamination throughout polymer layer). To eliminate this variable, it is recommended to use a focused ion bean (FIB) instrument to complete the slicing of these microscopes for future work.

As explained earlier, the proposed design aimed to create a 5% wt $CoCl_2$-PLGA shell layer and a 5% wt HA-PLLA core layer. Although the above EDS results show the presence of all desired elements, these elements are not purely in the desired layer location. It should be noted that for all samples (1-3), the core layer always had a higher concentration of HA and $CoCl_2$ present when compared to the shell layer. Further research was completed to better understand why both $CoCl_2$ and HA favored the core, PLLA layer. It was found that this distribution can be attributed to the difference of solubilities between the individual drugs (HA and $CoCl_2$) and the polymers (PLGA and PLLA) [10]. The solubility parameter is a means of predicating whether a compound will undergo dissolution in a given solvent and also a quantitative measure of that compound's polarity [21]. With $CoCl_2$ being polar (easily dissolves in water), the thought is that this compound will favor the more polar polymer, PLGA. Yet, only a small concentration of $CoCl_2$ remained in the PLGA shell (sample 2: 1.48 ± 0.95 wt% and sample 3: 0.15 ± 0.30 wt%, respectively) when compared to the amount of $CoCl_2$ present in the core (sample 2: 5.08 ± 0.96 wt% and sample 3: 2.63 ± 0.36 wt%, respectively). When applying the distribution theory, this indicates that the

difference in solubility parameters between $CoCl_2$ and PLLA is smaller when compared to solubility differences between $CoCl_2$ and PLGA. As for HA, this compound has a tendency to present hydrophobic characteristics at smaller concentrations (i.e. 2%) and hydrophilic characteristics at higher concentrations (i.e. 5%) [26]. For this study, a 5% (w/v) HA solution was loaded into the microsphere in hopes to create a PLLA core layer with 5% HA. Although the 5 wt% HA concentration was not achieved, more HA was present in the core than the shell, as desired. In addition, with Tihan's T.G.(2009) work in mind, striving for a 5% HA-PLLA core might be unachievable now knowing that HA will start to present more hydrophilic properties at this concentration which will lead to HA favoring PLGA (shell) over PLLA (core). Also, past studies have shown that the addition of hydroxyapatite can also aid with cartilage formation [16] and so having trace amounts of HA in the outer layer, in addition to $CoCl_2$, might be a design advantage for improving chondrogenesis.

3.3 Double-Walled Layer Identification

Double-walled microspheres fabricated with PLGA and PLLA mass ratio of 2:1, respectively, were analyzed after dissolution in acetone. Figure 9. shows optical microscope images of dissolution taking place during and after the addition of acetone to the surface of the, non-sectioned, microsphere. Also, Figure 10 shows the before and after dissolution on a cross-sectional view of a microsphere from sample batch 1. From both figures (9 & 10), its clear that the outer shell layer is what instantly dissolves upon the application of acetone. Based on the known solubility of PLGA and low-solubility of PLLA in acetone, the shell and core were identified as PLGA and PLLA, respectively.

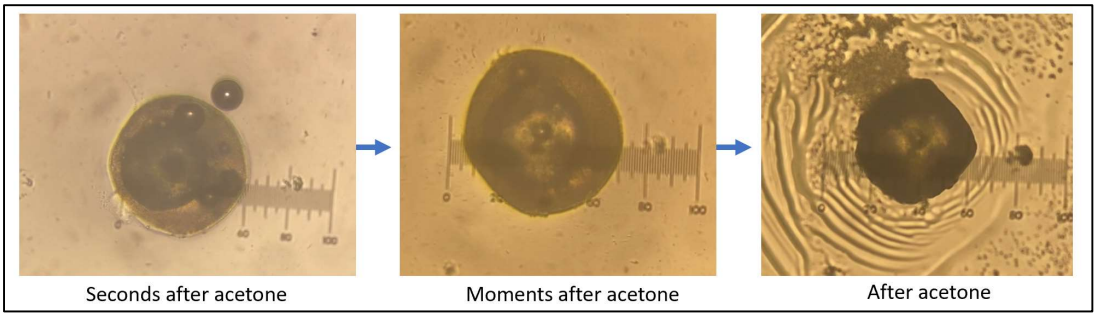

Figure 9. Example images of a double-walled microsphere, fabricated using the double emulsion technique, undergoing dissolution with acetone. The left and center images capture initial and moments after acetone application and the right image captures the final structure of the microsphere after dissolution.

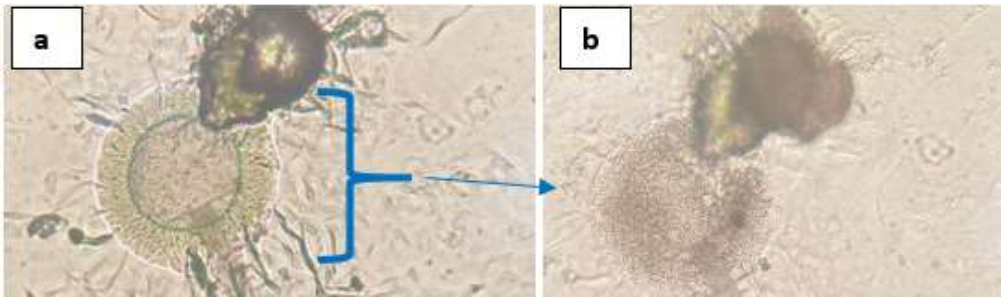

Figure 10. Cross-sectional view of microsphere from sample batch 1 undergoing dissolution with acetone where (a) shows the before and (b) the after.

As for layer size, it is clear that the shell layer is much thinner than the core layer. Visually this can be observed from Figure 6 (a-b) as shown above and Figure 11 (a-f) as shown below. These images show that the outer shell is anywhere between 50-150um and the core is anywhere between 200-600um. The large distribution seen in the core layer is due to the differences in total particle diameter, where the larger the particle size, the larger the core. In contrast, the distribution of shell layer thickness stayed relatively the same within both small and larger particles.

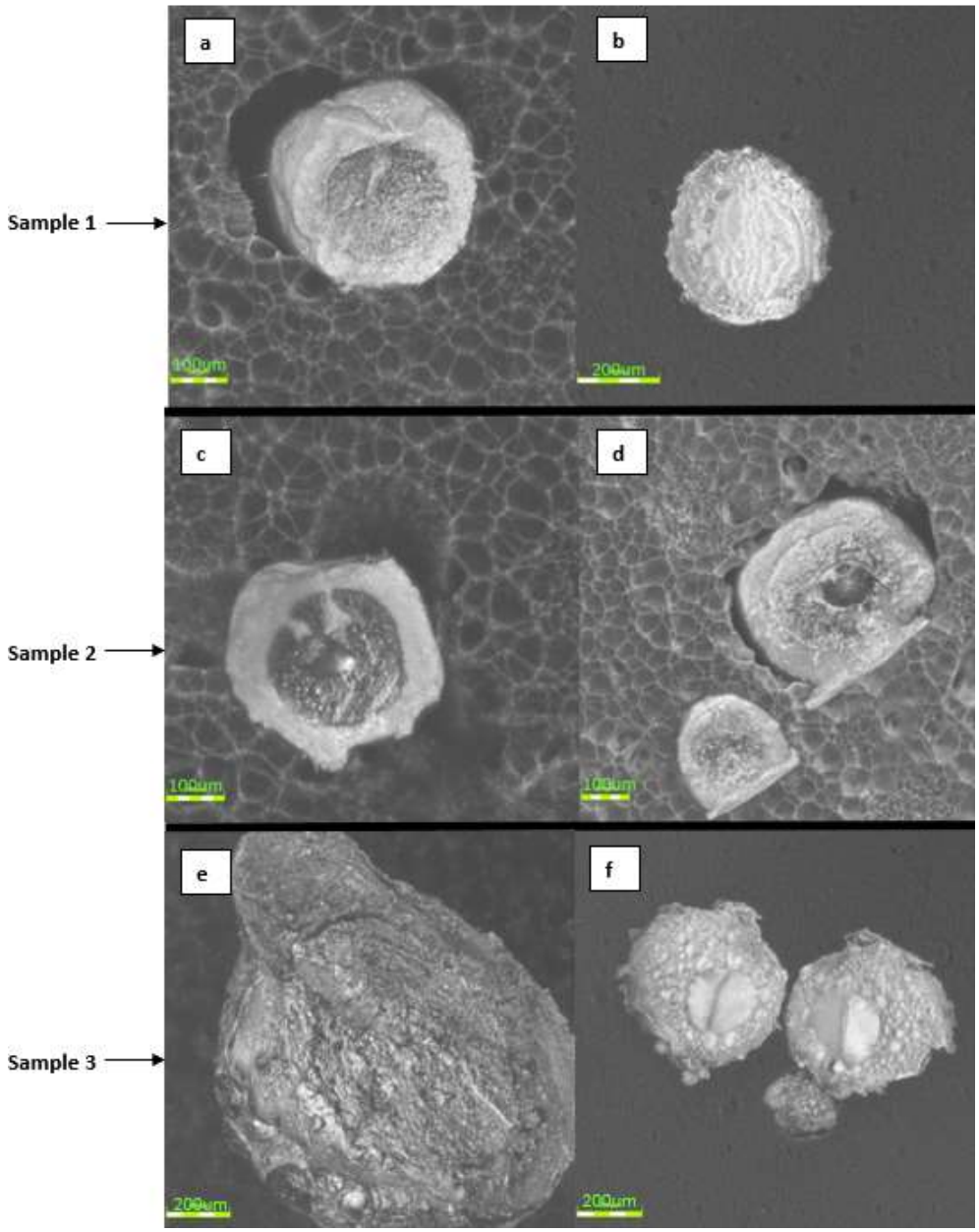

Figure 11. 3D laser microscope images all taken at 10x magnification of the cross-sectional views for each sample set, where sample 1 is shown in the first row (a-b), sample 2 in the second row (c-d), and sample 3 in the third row (e-f).

In addition to layer size and dissolution properties, the double emulsion structure of the microparticles is also captured in above figures Figure 9 and 11 (e-f). Double emulsions are liquid dispersion systems, in which the droplets of one dispersed liquid (emulsion, microemulsion, liposome, etc) are further dispersed in another liquid (water or oil), producing double layered

liquid droplets as shown [9]. These double walled structures have significant potential to serve as delivery vehicles [9] as well as 'entrapment reservoirs' for masking a substance or better controlling its release [10].

4. Conclusion

Fabrication of double-walled microspheres, loaded with both hydroxyapatite and cobalt(II) chloride, were developed and evaluated in this study. The proposed double-walled configuration aimed to have cobalt(II) chloride loaded in the PLGA shell layer and hydroxyapatite loaded in the PLLA core layer. Although these drugs were not located within the microsphere as desired, elemental analysis results concluded the presence of both hydroxyapatite and cobalt(II) chloride and selective dissolution methods concluded the correct location of the polymeric layers (PLGA as the shell and PLLA as the core). Overall, the purpose of this design is to allow direct injection of the microspheres to a large bone fracture site, where the $CoCl_2$ will initiate hypoxia, elevating the cellular response to regain vascularity and undergo chondrogenesis which then after degradation of this layer, the PLLA core layer will release hydroxyapatite to aid with bone formation. Future work will be needed to better understand the encapsulation efficiency (i.e. porosity) of this microsphere and the chondrogenesis and osteogenesis properties it may offer for improving the overall bone healing process for large fractures.

5. References

[1] Ansary, R. H., Rahman, M. M., Awang, M. B., Katas, H., Hadi, H., & Doolaanea, A. A. (2016). Preparation, characterization, and in vitro release studies of insulin-loaded double-walled poly(lactide-co-glycolide) microspheres. Drug Delivery and Translational Research, 6(3), 308-318. https://doi.org/10.1007/s13346-016-0278-y

[2] Bone Remodeling and Repair. (2020). In: LibreTexts.

[3] Cavaco, J. (2018). What to know about bone fracture repair. Healthline Media.

[4] Chengde, G., Shuping, P., Pei, F., & Cijun, S. (2017). Bone biomaterials and interactions with stem cells. Bone research, 5(4), 253-285. https://doi.org/10.1038/boneres.2017.59

[5] Cobalt Chloride: Colorful Moisture Detector. (2006). In: American Chemistry Council, Inc.

[6] David, F., Levingstone, T. J., Schneeweiss, W., Swarte, M., Jahns, H., Gleeson, J. P., & O'Brien, F. J. (2015). Enhanced bone healing using collagen–hydroxyapatite scaffold implantation in the treatment of a large multiloculated mandibular aneurysmal bone cyst in a thoroughbred filly. Journal of tissue engineering and regenerative medicine, 9(10), 1193-1199. https://doi.org/10.1002/term.2006

[7] Emma, M. M., Hayley, F., Owen, A., Zhenyu, J. Z., Pola Goldberg, O., & Liam, M. G. (2018). Influence of Cobalt Ions on Collagen Gel Formation and Their Interaction with Osteoblasts. ACS omega, 3(8), 10129-10138. https://doi.org/10.1021/acsomega.8b01048

[8] Eng Chew Tan, R. L., Chi-Hwa Wang. (2005). Fabrication of double-walled microspheres for the sustained release of doxorubicin. E. Inc.

[9] Garti, N., & Aserin, A. (2013). Double Emulsions. In T. Tadros (Ed.), Encyclopedia of Colloid and Interface Science (pp. 303-337). Springer Berlin Heidelberg. https://doi.org/10.1007/978-3-642-20665-8_26

[10] Garti, N., & Lutz, R. (2004). Recent progress in double emulsions. In Interface Science and Technology (Vol. 4, pp. 557-605): Elsevier B.V.

[11] Hilary Jane, A., Matthew John, D., Jugal, E., & Rein, E. (2016). ¬Mesenchymal Stem Cell Fate: Applying Biomaterials for Control of Stem Cell Behaviour. Frontiers in bioengineering and biotechnology, 4(MAY). https://doi.org/10.3389/fbioe.2016.00038

[12] Hu, D. P., Ferro, F., Yang, F., Taylor, A. J., Chang, W., Miclau, T., Marcucio, R. S., & Bahney, C. S. (2017). Cartilage to bone transformation during fracture healing is coordinated by the invading vasculature and induction of the core pluripotency genes. Development (Cambridge), 144(2), 221-234. https://doi.org/10.1242/dev.130807

[13] Höflinger, G. (2013). Brief Introduction to Coating Technology for Electron Microscopy. In: Leica Microsystems.

[14] Ki Hyun Kim , Z. A., Toshiaki Suzuki , Daisuke Shindo. (2010). Charging Effects on SEM/SIM Contrast of Metal/Insulator System in Various Metallic Coating Conditions (Materials Transactions, Issue. T. J. I. o. Metals.

[15] Kirkland, J. J. (1971). Modern practice of liquid chromatography. New York : Wiley-Interscience.

[16] Lee, J. B., Lee, S. H., Yu, S. M., Park, J.-C., Choi, J. B., & Kim, J. K. (2008). PLGA scaffold incorporated with hydroxyapatite for cartilage regeneration. Surface & coatings technology, 202(22-23), 5757-5761. https://doi.org/10.1016/j.surfcoat.2008.06.138

[17] Liang, X., Duan, P., Gao, J., Guo, R., Qu, Z., Li, X., He, Y., Yao, H., & Ding, J. (2018). Bilayered PLGA/PLGA-HAp Composite Scaffold for Osteochondral Tissue Engineering and Tissue Regeneration. ACS biomaterials science & engineering, 4(10), 3506-3521. https://doi.org/10.1021/acsbiomaterials.8b00552

[18] Liu, H., Li, D., Zhang, Y., & Li, M. (2018). Inflammation, mesenchymal stem cells and bone regeneration. Histochemistry and cell biology, 149(4), 393-404. https://doi.org/10.1007/s00418-018-1643-3

[19] Mariani, E., Pulsatelli, L., & Facchini, A. (2014). Signaling pathways in cartilage repair. International journal of molecular sciences, 15(5), 8667-8698. https://doi.org/10.3390/ijms15058667

[20] Matassi, F., Nistri, L., Chicon Paez, D., & Innocenti, M. (2011). New biomaterials for bone regeneration. Clinical cases in mineral and bone metabolism : the official journal of the Italian Society of Osteoporosis, Mineral Metabolism, and Skeletal Diseases, 8(1), 21-24.

[21] McCall, R. L., & Sirianni, R. W. (2013). PLGA nanoparticles formed by single- or double-emulsion with vitamin E-TPGS. Journal of visualized experiments : JoVE(82), 51015-51015. https://doi.org/10.3791/51015

[22] Müller, R., Abke, J., Schnell, E., Scharnweber, D., Kujat, R., Englert, C., Taheri, D., Nerlich, M., & Angele, P. (2006). Influence of surface pretreatment of titanium- and cobalt-based biomaterials on covalent immobilization of fibrillar collagen. Biomaterials, 27(22), 4059-4068. https://doi.org/10.1016/j.biomaterials.2006.03.019

[23] Sheen, J. R. (2020). Fracture Healing Overview. In V. V. G. . (Ed.). Treasure Island (FL): StatPearls.

[24] Sheikh, Z., Najeeb, S., Khurshid, Z., Verma, V., Rashid, H., & Glogauer, M. (2015). Biodegradable Materials for Bone Repair and Tissue Engineering Applications. Materials, 8(9), 5744-5794. https://doi.org/10.3390/ma8095273

[25] Sonnet, C., Simpson, C. L., Olabisi, R. M., Sullivan, K., Lazard, Z., Gugala, Z., Peroni, J. F., Weh, J. M., Davis, A. R., West, J. L., & Olmsted-Davis, E. A. (2013). Rapid healing of femoral

defects in rats with low dose sustained BMP2 expression from PEGDA hydrogel microspheres. Journal of orthopaedic research, 31(10), 1597-1604. https://doi.org/10.1002/jor.22407

[26] Tihan , T. G., Ionita, M. D., Popescu, R. G., & L ordachescu , D. (2009). Effect of hydrophilic–hydrophobic balance on biocompatibility of poly(methyl methacrylate) (PMMA)–hydroxyapatite (HA) composites (Materials Chemistry and Physics, Issue. Elsevier.

[27] Wang, W., & Yeung, K. W. K. (2017). Bone grafts and biomaterials substitutes for bone defect repair: A review. Bioactive materials, 2(4), 224-247. https://doi.org/10.1016/j.bioactmat.2017.05.007

[28] Yao, Q., Liu, Y., Tao, J., Baumgarten, K. M., & Sun, H. (2016). Hypoxia-Mimicking Nanofibrous Scaffolds Promote Endogenous Bone Regeneration. ACS Applied Materials & Interfaces, 8(47), 32450-32459. https://doi.org/10.1021/acsami.6b10538